Article

Characteristics of Cold and Hot Pressed Iron Aluminum Powder Metallurgical Alloys

Ahmed Nassef[1], W.H. El-Garaihy[2,*] and Medhat El-Hadek[3]

[1] Department of Production & Mechanical Design, Faculty of Engineering, Port-Said University, Egypt; nassef12@eng.psu.edu.eg

[2] Mechanical Engineering Department, Unizah College of Engineering, Qassim University, Kingdom of Saudi Arabia;

On leave from: Mechanical Engineering Department, Faculty of Engineering, Suez Canal University, Egypt; w.nasr@qu.edu.sa

[3] Department of Production & Mechanical Design, Faculty of Engineering, Port-Said University, Egypt; melhadek@eng.psu.edu.eg

* Correspondence: w.nasr@qu.edu.sa; Tel.: +966-55-110-8490

Abstract: Iron powders having average particle sizes of ~40 μm are mechanically mixed thoroughly with aluminum powders ranging from 1 to 10 in wt. %, with an average particle size of ~10 μm. Two different powder metallurgical techniques, cold and hot pressing, are used to study the effect of the additive element powder on the mechanical properties, wear properties, and the microstructure of the iron based alloys. The hot pressing technique was performed at a temperature reaching up to 500°C at 445.6 MPa. The cold pressing technique was performed at 909 MPa at room temperature. By increasing the Al content to 10 wt. % in the base Fe-based matrix, the Brinell hardness number was decreased from 780 to 690 and the radial strength from 380 to 228 MPa with reductions of 11.5% and 40%, respectively. Improvement of the wear resistance with the increase addition of the Al powder to the Fe matrix up to 5 times was achieved, compared to the alloy without Al addition for different wear parameters namely instead of; wear time and sliding speed.

Keywords: Iron Aluminum Alloys; Cold/ Hot PM; Compressibility Factor; Wear Resistance.

1. Introduction

Some of the advantages of powder metallurgy (PM) alloys include minimum cost, high flexibility, ability to be shaped into complicated products and use metastable structures, wide-ranging reinforcement levels [1, 2]. Powder metallurgy technique can be used to reach homogeneity in the matrix distribution of the reinforcement without extreme reaction of matrix–reinforcement, which causes a problem in some techniques; such as, stir casting or squeeze infiltration of the reinforcement in the molten matrix, under a dry and protective atmosphere. This is a result of the development of transient liquid phase throughout the sintering process. The liquid phase penetrates between the matrix grain boundaries, in case of satisfactory wetting of the matrix by the melt.

Metal matrix composites (MMCs) containing nonmetallic particulates tend to ameliorate the wear and mechanical properties, through the creation of constraints to the distortion of the material during the mechanical working [3, 4]. Perhaps the greatest advantage of PM techniques mendacities in the development of special material structures and the possibility of combining different components widening the field of application of the PM materials [5, 6]. Iron (Fe) is renowned for its strength and low price but it is very heavy in weight. To make use of it in scenarios that demand light weight without resorting to buying expensive stronger materials such as titanium (Ti), it is often alloyed with aluminum (Al) which is light and cheap. The mixture of iron and aluminum usually includes a sprinkling of manganese to make it less brittle. Brittle intermetallic compounds can form poor ductility alloys at room temperature, which would limit their usage as they are

difficult to process into useful shapes, such as plates and tubes [7]. Using strengthening second phase control, Fe–Al alloys can be effectively hardened by controlling aluminum morphology and dispersion, in the iron based alloy [7]. Phase identification for Fe–Al alloys was initiated by the early effort of Koster and Tonn in 1933s [8] on the equilibrium phases. James [9] showed that subject to the temperature and chemistry, there are five stated equilibrium phases for Fe–Al alloys namely: γ-austenite, α-ferrite, and β-Mn. The compound Fe–Al is present in a variety of compositions, mostly on the iron rich side of stoichiometry. It is characterized by its ordered body centered cubic (BCC) structure [10]. It has been an important subject of interest, commercially, due to its outstanding oxidation resistance, acceptable strength at high temperatures reaching ≈ 530°C, and minimum density (5.76–6.32 g/cm^3 depending on Fe/Al ratio) when related to other iron based alloys utilized in market [11]. Iron aluminide intermetallic of Fe_3Al and FeAl possess attractive properties for application, such as structural materials at high temperatures in aggressive environments [12, 13]. Tanaka et al [14] investigated Fe–Al superalloys with an 11.5% Al content; they have a relatively high solvus temperature with high hardness when aged at 600°C. Although the agreement with the experimental results was not optimum, Carbon and Al contents had a positive influence on the constituent phase for the stability of the κ carbide phase; however, the experimental results were not in an optimum agreement with this finding [15].

Since the early 2000s the interest in the Fe–Al alloys for automotive applications has been aggravated in Europe and Japan [16], as the demand arisen on the light of producing durable automobiles. Due to the wide difference between the melting temperatures of iron (~1540°C) and aluminum (~660°C), the sintering of Fe–Al was; in fact, liquid phase sintering. As the sintering treatment is carried out above the melting point of the aluminum, the liquid phase may be stable or transient at the usual sintering temperatures, approximately 30 wt. % Al being soluble in α–Fe [16]. Although lightweight steel has an apparent shape of simplicity; however, it is very complex in its underlying metallurgical issues, which is associated to its potential to have structures; such as, austenitic, ferritic, or even multiphase. TRIPLEX is a multiphase steel described in literature by Frommeyer and Brux [17], which is a Fe–Al–Mn–C lightweight alloy characterized by having high ductility, strength, and a multiphase structure. The three major phases of TRIPLEX steel have a matrix phase composition of austenite with volume percentages of ferrite lying from 5 to 15; moreover, finely dispersed nano size κ-carbides all over the austenite with volume percentages less than 10. Frommeyer and Brux [17] added Al up to 12 wt. % and reported a 1.5% linear relationship with the decrease in density per adding 1 percent of Al weight. Their distinctive of Fe–28Mn–12Al–1C alloy went to be tested mechanically in a uniaxial tensile test, which was accomplished at strain rate of 10^{-4} s^{-1} and room temperature. The results showed that ultimate tensile strength reached 1000 MPa, yield strength of 730 MPa, and total elongation of 55%. Sutou et al [18] lately stated that by Al addition for more than 11 wt. %, the Fe–Al alloy cold workability has been depreciated to ~10%.

Material's wear resistance is vital to designers as it is linked to surfaces' interactions; particularly, mechanical action of the opposite surface leading to material's elimination and deformation. The wear analysis of Fe–Al alloys, with Fe being the base matrix, is deficient in the literature [19, 20]. Perhaps one of the inimitable studies on the worn surfaces for Fe–Al alloys was reported by Xu et al [21], where the Fe–Al alloys were found to exhibit high wear resistance. They found that with augmenting the load, a slight reduction in friction takes place, as a result of increased friction contact temperature and the bigger areas on the worn surface of the oxidized film, which act as a solid lubricant. At the deeper position below the surface, augmenting the load increases the shear stress; thus, aggravating the wear as aluminum affects the flexibility of the alloy [21]. Kim et al [22] stated that the increase in wear rate of the iron-aluminides containing 25, 28 and 30 wt. % aluminum is associated with the increase of wear sliding speed and applied normal load; moreover, wear resistance of the aluminides decreased with augmenting the aluminum contents, where a ductile material's wear behavior linked to plastic deformation was discovered under SEM observations at worn surfaces of the iron-aluminides [22].

Mechanical alloying using two PM processing techniques, hot and cold pressed, were used for the production of strengthened Fe-based alloys, having additives of Al ranging within 1, 2, 3, 5 and

10 in wt. %. The procedure is based on a blending process in a hot and cold pressed attrition for elemental powders along with master alloy, which are ball milled in a protective and dry atmosphere. The present work aims to control and optimize the production of processing parameters, through suitable compaction die design to get dense PM parts, and study the influence of the production methods on the structure density, hardness and wear properties of the iron alloys containing aluminum dispersions.

2. Experimental Procedures

A commercial pure iron powder reduced by hydrogen, with 99.1% purity, average particle size of ~40 μm, molecular weight of 55.845 g/mol, and a density of 7.845 g/cm^3, was mechanically mixed thoroughly with aluminum powders as reinforcement, with 99.9% purity, average particle size of ~10 μm, mesh no. of 80, molecular weight of 26.98 g/mol, and a density of 2.9 g/cm^3. The iron metallic powder was obtained from CNPC powder-Canada, whereas the aluminum metallic powder was obtained from ALDRICH-Germany. The two metallic powders were mechanically mixed to study the effect of the aluminum addition on the mechanical and the wear properties of the iron based alloys. The weights of powders were calculated, to manufacture specimens of iron based alloys with Al additives ranging within 1, 2, 3, 5 and 10 in wt. %.

An arrangement of single acting piston cylinder, at room temperature, was adopted to perform the compaction process, as shown in Figure 1. The arrangement aimed at obtaining dimensions of the green compact of a 30 mm in diameter of and a height of 50 mm. The temperature was maintained at the desired level with a tolerance of ± 5 °C. A pressing pressure of 909 MPa with cold pressing was calculated, with the assumption that the cross section area of the compact is equal to the cross section area of the die [8];

$$P = \frac{4\ F}{\pi\ D^2}$$

Where, P is the pressing pressure (MPa), F is the load (N) and D is the die diameter (mm). Various temperatures of molds were experienced with a maximum of 500°C, while maintaining a pressure of 445.6 MPa with hot pressing and fixed cross head velocity of 2 mm/min. The setup was; consequently, heated then maintained for half an hour at the chosen temperature, for the sake of reaching temperature homogeneity all over the powder alloy. Afterwards, a reduction of the forming pressure was taken place for all tested hot components. Consequently after the compact operation, samples were enclosed using foils of aluminum surrounded with a graphite powder to shield its surface from the atmosphere during the sintering process, avoiding any potential reaction with oxygen and nitrogen. The cold and hot compacts were then sintered at 800°C for one hour before being; finally, furnace cooled. The radial strength of the sintered pressed samples was determined using ASTM B939-15 standards [23 and 24], whereby annular compacts are crushed; the radial strength was calculated as;

$$RS = \frac{L_c(D-T)}{h.T^2}$$

where RS is the radial strength (MPa) , L_c is the crushing load at failure (N), T is the compact wall thickness (mm), D is the outer compact diameter (mm), and h (mm)is the height of the compact mass of specimen and its cross section were constant. The final compact height h_c was calculated as follow [25];

$$h_c = \frac{h_o(RD)_i}{(RD)_C}$$

Where h_o is the initial compact height after 1 ton pressing, $(RD)_i$ is the initial relative density, the $(RD)_c$ is the compact relative density after sintering. The initial relative density can be calculated as follow;

$$(RD)_i = \frac{mass/(h_o.\frac{\pi}{4}.D^2)}{\rho_c}$$

Where ρ_c is the compact density (g/cm³). The compact relative density after sintering can be calculated from equation (5), and the compact relative density is calculated according to equation (6);

$$(RD)_c = \frac{\rho_m}{\rho_c}$$

$$\rho_c = \frac{w_1\% + w_2\% + \cdots + w_n\%}{\sum_{i=1}^{n}(w\%/\rho)_i}$$

Where ρ_m is the measured compact density, w_i % is the weight fraction of element i, ρ_i is the density of element i, and n is the element's number. The compressibility factor C_f of the metal powder was calculated using equation (7) [26, 27];

$$C_f = \frac{\rho_c - \rho_o}{P^{1/3}}$$

Where ρ_o is the apparent density of the powder (g/cm³), respectively, and P is the applied pressure. The porosity was calculated after the sintering process for each specimen according to; $\theta = 1-(RD)_c$. Metallographic specimens were then prepared by polishing and etching done mechanically in a solution of (20 ml HNO_3+10 ml H_2SO_4+20 ml H_2O) then cleaned by a solution of (10 ml NaOH +100 ml H_2O). Brinell hardness was measured using a 5 mm ball hardened diameter, at 750 Kg load for 15 sec.

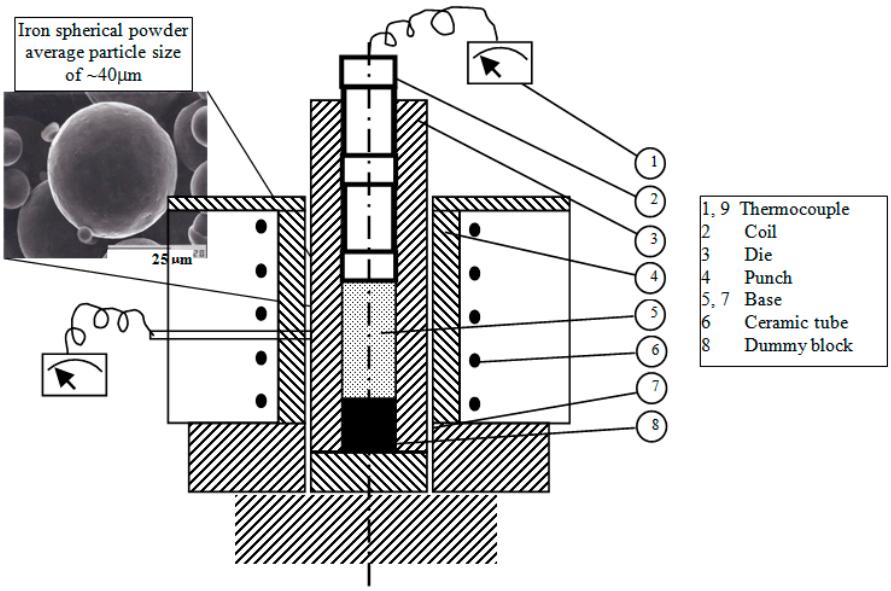

Figure 1. The setup of die of PM pressing technique.

3. Results and Discussion

3.1. Microstrautral Optical Investigations

The microstructure investigation on the Fe-based alloys was conducted using a Jeol 5400 scanning electron microscope (SEM) unit. It is connected to an EDS detector attachment used to detect various particle properties after the fabrication process. Particle size, morphology, shape, and agglomeration are obtained. The aluminum contents ranging within 1, 2, 3, 5 and 10 in wt. % were added to the iron powder and then produced using cold and hot pressing techniques. The measurements were carried out three times under the same conditions, to ensure repeatability. The achieved theoretical density after the sintering of the cold pressing samples was found to be 95% from the solid density.

3.1.1. *Cold Pressed*

Figure 2 shows the optical micrographs of the cold pressed (CP) Fe-based alloys with aluminum contents ranging within 1, 2, 3, 5 and 10 in wt. % at a pressing pressure of P = 909 MPa followed by a sintering process of at 800°C for one hour followed by furnace cooling process. The pure iron specimens were sintered at higher temperature up to 900°C for one hour followed by furnace cooling process. The sintering process resulted in reducing the specimen's porosity due to coalescence processes between powders and eliminating the specimen's pores. It creates new solid-solid interfaces, distinctive with their lower energy and reduced free energy occurring on sintering one micrometer particles to a 1 cal/g decrease. On a microscopic scale, varying pressure and free energy across the curved surface affect obviously the material transfer. In other words, the increase of small particle size with high curvature results in augmenting the differences in free energy across the curved surface [28 - 32].

It is noticed in Figures 2 (c and d) that a fine dispersion of precipitates occurs at the grain surface. The uniform distribution of the Fe and Al in the homogenous structures was noticed in alloys with Al additions of 2 or 3 in wt. % compared to the rest of the Fe-based matrix alloys. Rapid growth of the iron grains during sintering was observed as one of the limitations of the cold pressed PM method. Also, it should be reported that surface cracks in the Fe–10 wt. % Al alloy were encountered.

3.1.2. Hot Pressed

Hot pressing (HP) technique followed by heat treatment was performed to avoid the limitations observed under the cold compaction technique. The Fe–5 wt. % Al and Fe–10 wt. % Al alloys were selected to conduct the hot pressing process. The specimens were pressed at 445.6 MPa, under a pressing temperature ranging from 200 to 500°C, followed by a heat treatment for one hour duration, at a temperature of 800°C, going to furnace cooling conditions of 1°C/min [6]. The temperature was then held at the same level with a tolerance range of ± 5°C. Figure 3 shows the microstructure of the hot pressed Fe–5 wt. % Al alloys samples with various pressing temperatures (TP).

The hot pressed samples followed by heat treatment showed very fine and uniformly dispersed Fe–5 wt. % Al alloys, precipitated around the grain boundaries, with an average particle size of ~5 μm in the Fe-based matrix. Figure 4 shows a homogenous structure of Fe–10 wt. % Al alloy, which was obtained with heat treatment at 800°C for one hour and furnace cooling as the cracks after the sintering process had disappeared.

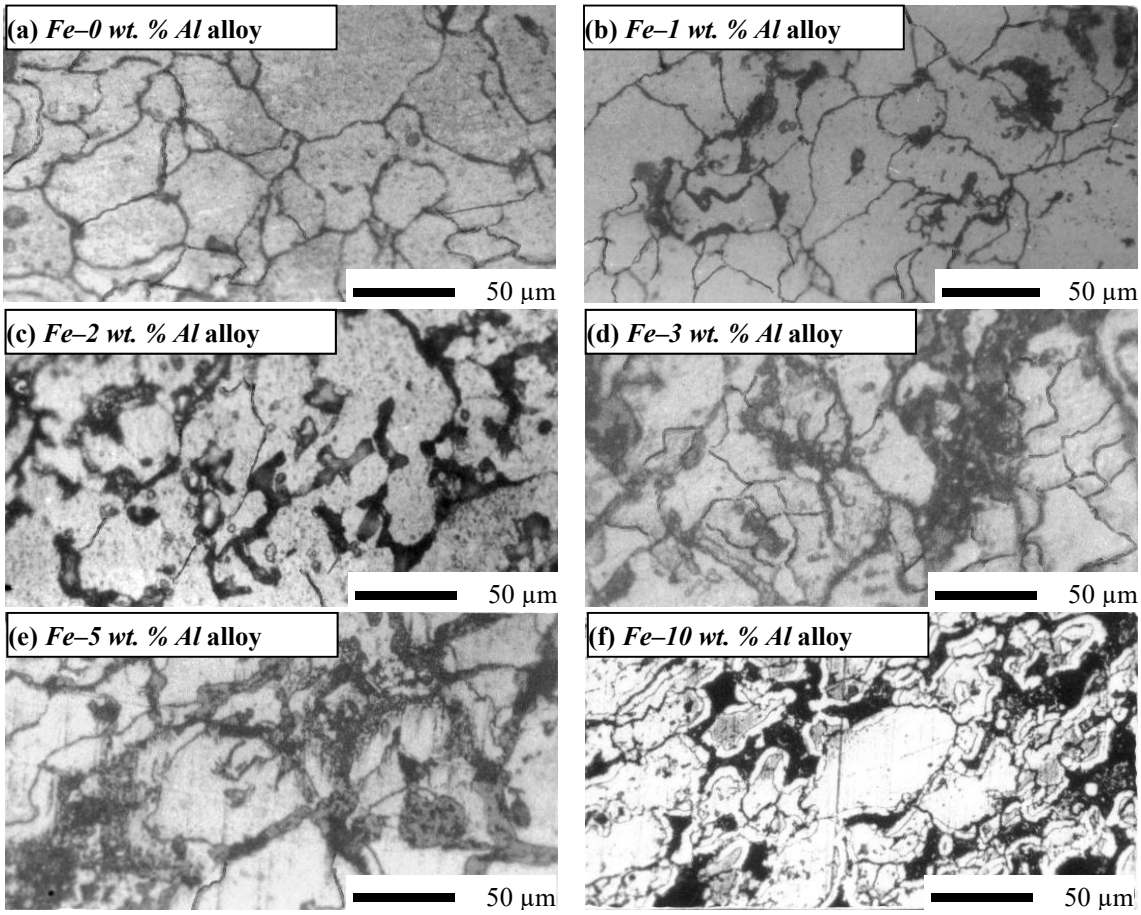

Figure 2. Optical micrographs of cold pressed Fe-based alloys with Al contents ranging from 1 to 10 wt. % at pressure of P_P = 909 MPa followed by sintering process of at 800°C per one hour at constant furnace cooling conditions.

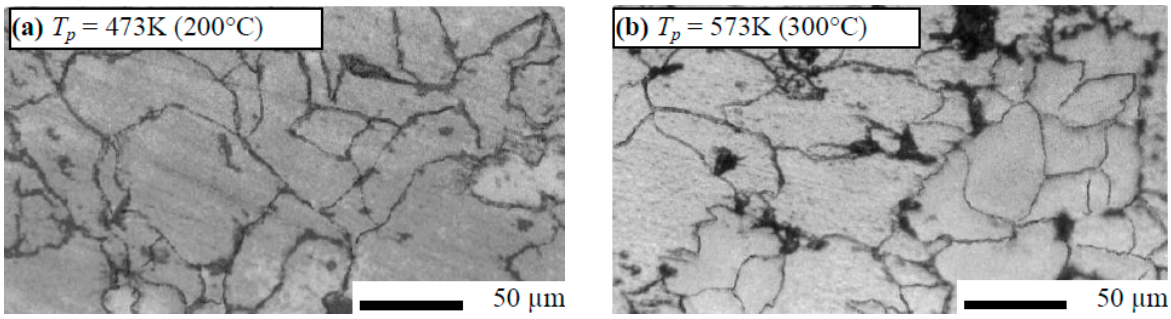

(a) (b)

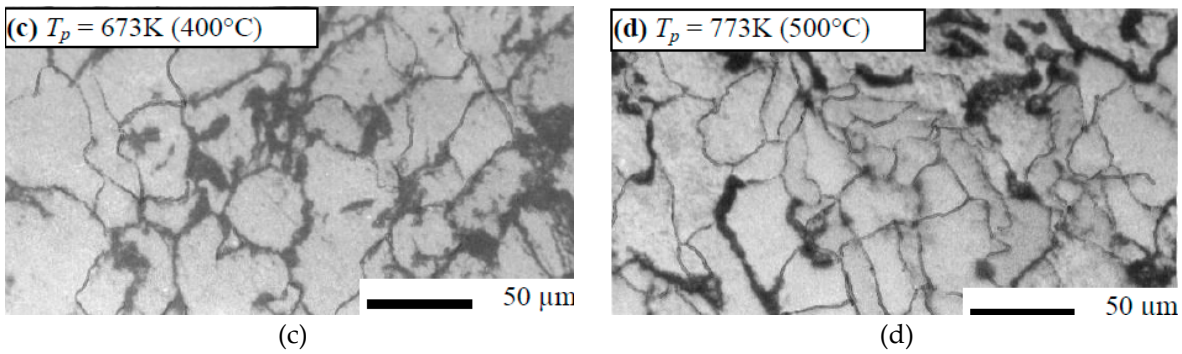

Figure 3. Microstructure of hot pressed and heat treated Fe–5 wt. % Al alloys at four various Tp.

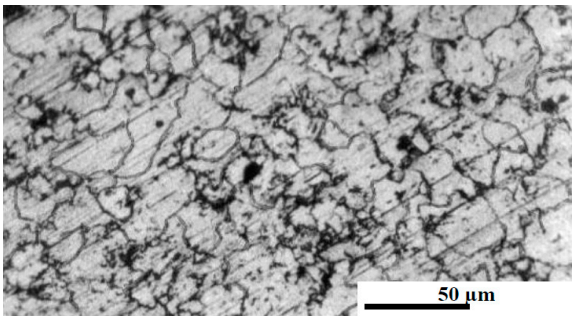

Figure 4. Microstructure of hot pressed Fe–10 wt. % Al alloy with heat treatment at 800°C for one hour and furnace cooling conditions.

3.2. Hardness and Radial Crushing Strength

A minimum of ten readings were taken for the different cases to guarantee consistency of the Brinell hardness values crosswise the surface of material; the average of the readings is presented in Table 1. Radial strength tests were performed using an Instron 8562 universal mechanical tester under quasi static loading and a strain rate of 8×10^{-5} ±5% s^{-1}, at laboratory temperature. Specific dimensions of cylindrical specimens were set at a 30 mm diameter and a height of 50 mm. The samples went through deformation until crashed. Three similar samples were arranged for every test situation and subjected to the same loading conditions, to guarantee homogeneity and consistency. The average test value of all the three samples of the radial crushing strength was reported in Table 1. By increasing the Al content to 10 wt. % in the base Fe-based matrix, the Brinell hardness number was reduced from 780 to 690 and the radial strength from 380 to 228 MPa, as shown in Table 1. The hardness and radial strength of Fe–10 wt. % Al alloy was considerably lower than that of the Fe–0 wt. % Al alloy with a reduction of 11.5% and 40%, respectively. This reduction was due to a combined effect of the Fe-base matrix by the addition of Al powder, which causes a precipitation strengthening of the alloy matrix.

Table 1. Brinell hardness number and the radial strength for Fe-based alloys with various Al additions.

***Al* content in *Fe*-based alloys wt. %**	**Brinell Hardness Number**	**Radial Strength *MPa***
0	780	380.44
1	751	369.78
1.5	735	344.67
2	722	310.11
2.5	714	270.23
3	705	245.11

5	698	235.14
7.5	691	230.21
10	690	228.43

The Al phase was dispersed in many pools or lakes, present in the cylindrical crashed Fe-base alloy samples. Continuous crystallization during the plastic deformation resulted in extraordinary hardness. The cold pressed Fe–based alloys with the addition of Al were detected to go through mechanically induced fine crystallization, as presented in the SEM Figure 5 (a) for Fe–5 wt. % Al and (b) for Fe–10 wt. % Al alloys, respectively. Fine crystal precipitation in the Fe–Al alloys was detected within vein protrusions, on the surface of compression fracture, and all along the paths of the rough crack propagation; additionally, within shear bands resulting from bending [33]. As a result, more tendencies towards plastic deformations take place and less critical shear stresses are resulted.

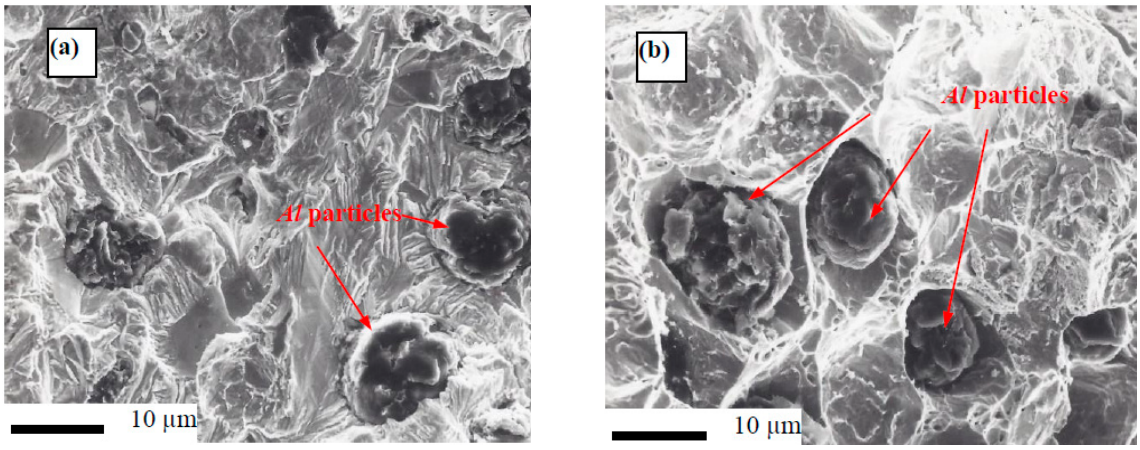

(a) (b)

Figure 5. SEM micrographes the rough fracture surface morphology of the CP Fe-based (a) for Fe–5wt.%Al, and (b) for Fe–10 wt. % Al alloys, respectively.

The effect of the pressing temperature on the density, relative density, and compressibility factor of the Fe–5 wt. % Al alloy is shown in Figure 6a. The compact density and porosity are affected by the pressing temperature, as shown in Figure 6b; in other words, the density increases by increasing the temperature, which leads to porosity minimization. Higher relative density (RD) was reached for hot pressing Fe–5 wt. % Al alloy samples to ~95% from the solid density. Compressibility was used to indicate that the density of the powder had increased by a given pressure. By increasing the pressing temperature, the compressibility factor of the Fe–5 wt. % Al alloy was increased, as shown in Figure 6b, where augmented relative density and porosity reduction of the compact were detected. The porosity has already been presented in the green compacts. The pores formed during the sintering process were causing a different type of porosity, due to the formation of transient liquid phase during sintering, where the liquid phase penetrates into the matrix grain boundaries. Due to satisfactory wetting of the matrix by the melt, the alloying element particles replaced the pores and the homogenization leads to an overall expansion of the material during sintering.

The hot pressed compact quality was identified by the correlation with the three process parameters namely: time, pressure, and temperature. These variables had a major effect on the microstructure, physical properties, dimensional accuracy, and surface condition of the product. For the powders heated to low temperatures, pressure had the same effect as in cold pressing. Particles were brought closer together and were rotated and deformed, sheared, or fractured. At elevated temperatures, plastic deformation becomes the dominant mechanism. The liquid phase was formed at the hot pressing temperature and consolidation was further enhanced, by the isostatic action of the compressive stresses on the compact inside the dies [26, 34, and 35]. Additionally, diffusion rates were increased through enhancing the liquid phase and densification, by good wetting between liquid and solid components of the alloy system.

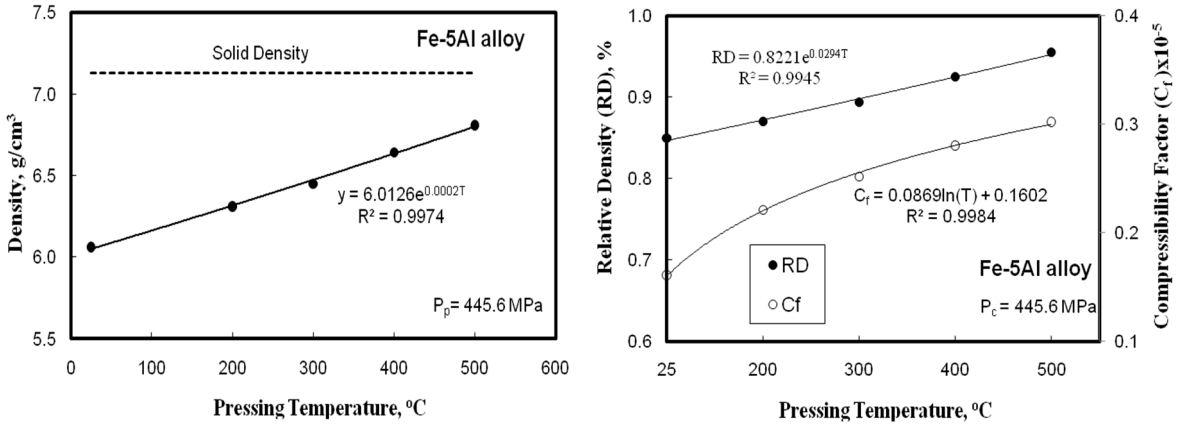

(a) (b)

Figure 6. (a) the effect of the pressing temperature on the compact density and porosity, and (b) the effect of pressing temperature on the compact relative density (RD) and compressibility factor (Cf), for Fe–5 wt. % Al alloys respectively.

3.3. Wear Resitance

Dry sliding wear tests were done using pin-on-disc apparatus for the Fe-based alloys with aluminum contents of 1, 2, 3, 5 and 10 in wt. % compared to stainless steel. Cylindrical specimens with 30 mm in diameter and height of 50 mm were slid against a rotating steel disc at various sliding speeds as f
steel using
wear press
wear rate v
distance. M
of ±0.05g. I
pressing Fe
calculated

$$= \frac{Wl}{\rho * S_s * t}$$

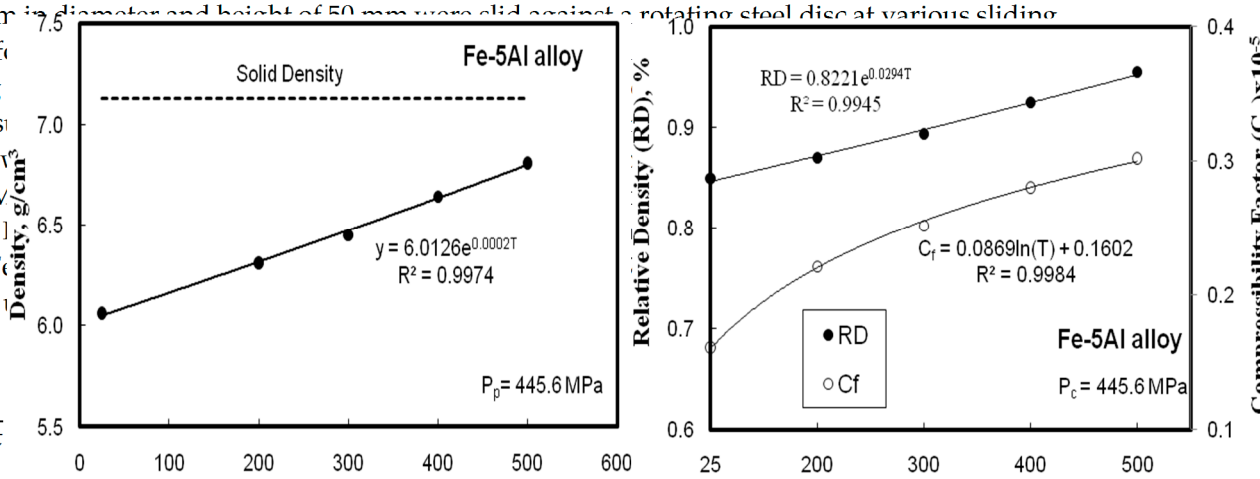

Where Wl is the weight of the sliding specimen, ρ is the production density o the sliding speed, and t is the wear time.

The wear rate of Fe-base alloys with Al powder addition was much less than the one without addition of Al element to the iron base matrix, at various wear parameters. The wear rate at higher speed was much less than the one at lower sliding speed as shown in Figure 7b. Comparison of the wear behavior for the alloys produced, using different powder metallurgy techniques, is shown in Figure 7a, and b. A significant reduction in wear rate was obtained using Fe-Al alloys in comparison with the Fe–0 wt. % Al alloy. While the addition of Al element powder to the Fe-base matrix causes a reduction in the wear rate, which increased the wear resistance up to 5 times compared with the alloy without Al addition, as shown in Figure 7a and b.

Preprints (www.preprints.org) | NOT PEER-REVIEWED | Posted: 3 April 2017 doi:10.20944/preprints201704.0003.v1

Peer-reviewed version available at Metals 2017, 7, , 170; doi:10.3390/met7050170

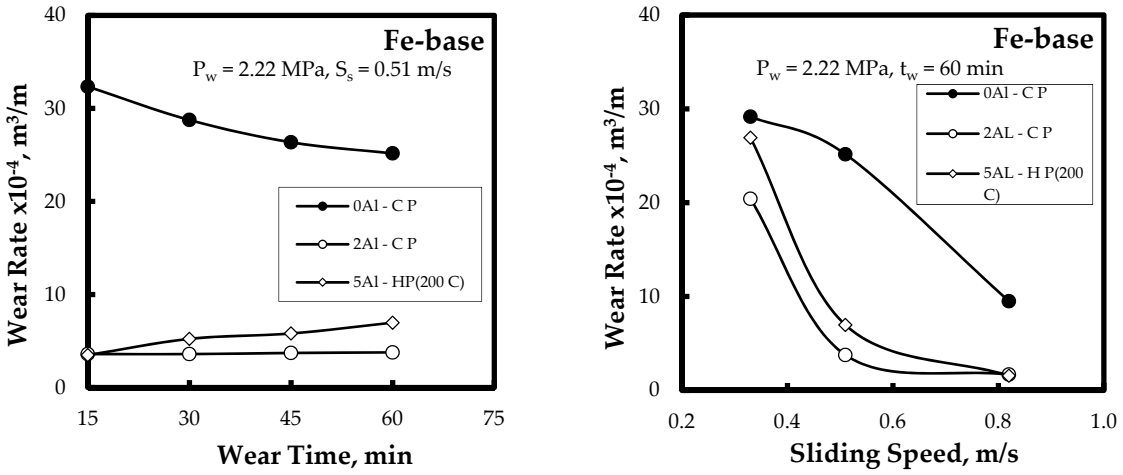

(a) (b)

Figure 7. The effect of wear parameter for Fe-base alloys different PM technique on (a) wear time, and (b) sliding speed for Fe–0 wt. % Al (CP), Fe–2 wt. % Al (CP), and Fe–5 wt. % Al (HP at 200ºC) alloys, respectively.

Figure 8 shows the wear behavior of Fe–2 wt. % Al alloy (cold pressing) under different wear pressures. It is clear that increasing the wear pressure resulted in increasing the materials loss, which is a regular known behavior for a vast variety of metals and all alloys, regarding wear reactions. Hardness plays the predominant role at light wear process, while plasticity has big role at heavy operating conditions [39]. Heat generated due to the friction at high speed affects the microstructure, reduces hardness, and causes thermal stresses in the alloy matrix. As a result, a change in the wear mechanism takes place from abrasive to adhesive wear. Therefore, the worn surface layer is removed and the friction surface is protected from more wear and motion is facilitated, due to the relatively low value of shear strength [40, 41].

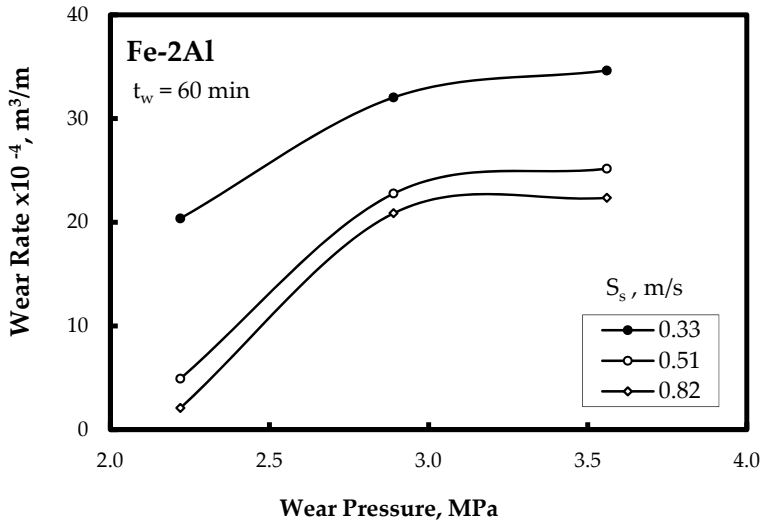

Figure 8. The effect of wear pressure for Fe–2 wt. % Al alloy (CP) on the wear rate.

The relation between the wear rate and wear time of the Fe–5 wt. % Al alloy pressed at different pressing temperatures is shown in Figure 9a, while Figure 9b shows the relation between the wear rate and the sliding speed of the Fe–5 wt. % Al alloy pressed at the same pressing temperatures. The higher wear rate of hot pressed specimen (300°C) was due to its coarsening structure and the pressing temperature, which was not enough to precipitate the Fe-Al alloys hard phase around the grain boundaries. The lower wear rate of hot

pressed specimens at 400 or 500°C could be attributed to its finer grain structure and spheroidization of the pores after the sintering process. In general, there was a decrease in the wear rate for the hot pressed Fe-Al alloy sampled at 200°C and an increase in the wear rate with increasing the hot pressing temperature, under the same wear parameters, as presented in Figure 9a and b. This finding could be attributed to the decrease of the residual porosity by increasing the pressing temperature.

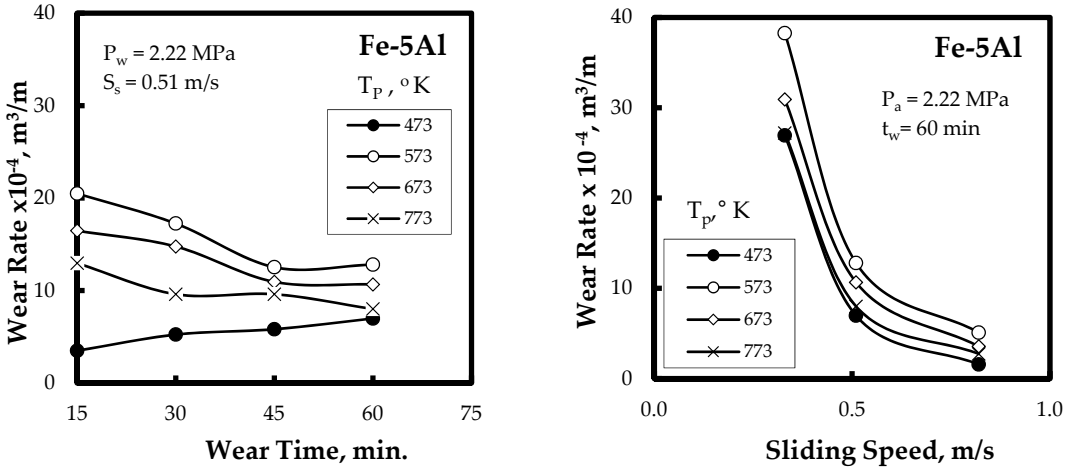

(a) (b)

Figure 9. The effect of wear parameters for Fe–5 wt. % Al alloy at different pressing temperature on (a) wear time, and (b) sliding speed, respectively.

5. Conclusions

Based on the findings of this study, the following conclusions could be summarized:

1. Under laboratory conditions and without the use of lubricant or binder, it was possible to produce Fe-Al with Al additives ranging within 1, 2, 3, 5 and 10 in wt. % alloys, using two powder metallurgy techniques namely, cold and hot pressed having comparable theoretical density and properties of the solid metals. Uniform distribution of dispersed phase inside the alloy structure was obtained.

2. By augmenting the Al content to 10 wt. % in the base Fe-based matrix, the Brinell hardness number was reduced from 780 to 690 MPa and the radial strength from 380 to 228 MPa, with a reduction of 11.5%, and 40%, respectively. The reduction of the compressibility factor of hot pressed powder alloys was detected with increasing the hot pressing temperature up to 500°C.

3. Improvement of the wear resistance was observed, with augmenting the Al powder to the Fe matrix up to 5 times compared with the alloy without Al additions for different wear parameter namely; wear time, and sliding speed. This was also detected for the different PM technique.

4. The hot compact of Fe-Al alloys of about 95% theoretical density can be obtained from the metal powders, by employing a pressure of about 445.6 MPa and temperature of 500°C. These alloys had higher density, better wear resistance, and homogenous structure than the parts produced by separate compaction and sintering obtained after elemental powders were added.

Author Contributions: All authors have equal contributions. Authors have no competing financial interests. The authors also declare no conflict of interest.

References

1. Caballero, E. S.; Cintas, J.; Cuevas, F.G.; Montes, J.M.; Ternero, F. Influence of Milling Atmosphere on the Controlled Formation of Ultrafine Dispersoids in Al-Based MMCs. Metals **2016**, 6, 224, 1-9. DOI: 10.3390/met6090224.
2. Luka, F.; Vilemova, M.; Nevrla, B.; Klecka, J.; Chraska, T. Properties of Mechanically Alloyed W-Ti Materials with Dual Phase Particle Dispersion. Metals **2017**, 7, 3, 1-10. DOI: 10.3390/met7010003.
3. Chen, C.L.; Lin, C.H. A Study on the Aging Behavior of Al6061 Composites Reinforced with Y_2O_3 and TiC. Metals **2017**, 7, 11, 1-8. DOI: 10.3390/met7010011.
4. El-Hadek, M. A. Numerical simulation of the inertia friction welding process of dissimilar materials. Metall. Trans. B **2014**, 45(6), 2346-2356. DOI: 10.1007/s11663-014-0148-2.
5. Nassef, A.; El-Hadek, M. Mechanics of hot pressed aluminum composites. Int. J. Adv. Manuf. Technol. **2015**, 76 (9-12), 1905-1912. DOI: 10.1007/s00170-014-6420-4.
6. Nassef, A.; El-Hadek, M. Microstructure and Mechanical Behavior of Hot Pressed Cu-Sn Powder Alloys. Adv. Mater. Sci. Eng. 2016, **2016**, 1-10 . DOI: http://dx.doi.org/10.1155/2016/9796169.
7. Kim, S. H.; Kim, H.; Kim, N. J. Brittle intermetallic compound makes ultrastrong low-density steel with large ductility. Nature **2015**, 518(7537), 77-79. DOI: 10.1038/nature14144 .
8. Köster, W.; Tonn, W. The Iron Corner of the Iron-Manganese-Aluminium System. Arch. Eisenhuettenwes **1933**, 7, 365-366 .
9. James, P. J. Precipitation oF The Carbide-FEMN-3 ALC IN AN Iron-Aluminium Alloy. Journal of Iron Steel Insturial **1969**, 207(1), 54-57.
10. Furushima, R.; Katou, K.; Shimojima, K.; Hosokawa, H.; Mikami, M.; Matsumoto, A. Effect of η-phase and FeAl composition on the mechanical properties of WC–FeAl composites. Intermetallics **2015**, 66, 120-126. DOI: 10.1016/j.intermet.2015.06.023.
11. Amaya, M.; Romero, J. M.; Martinez, L.; Pérez, R. Mechanical Properties of Spray-Atomized FeAl40 at.% Al Alloys. In Materials Characterization **2015**, 199-207. Springer International Publishing. DOI: 10.1007/978-3-319-15204-2_20.
12. Trotter, G.; Baker, I. The effect of aging on the microstructure and mechanical behavior of the alumina-forming austenitic stainless steel Fe–20Cr–30Ni–2Nb–5Al. Mater. Sci. Eng. A **2015**, 627, 270-276. DOI: 10.1016/j.msea.2014.12.072.
13. Zamanzade, M.; Barnoush, A.; Motz, C. A Review on the Properties of Iron Aluminide Intermetallics. Crystals **2016**, 6(1), 10. DOI: 10.3390/cryst6010010.
14. Tanaka, Y.; Kainuma, R.; Omori, T.; Ishida, K. Alloy Design for Fe-Ni-Co-Al-based Superelastic Alloys. Materials Today: Proceedings **2015**, 2, S485-S492. DOI: 10.1016/j.matpr.2015.07.333.
15. Ikeda, O.; Ohnuma, I.; Kainuma, R.; Ishida, K. Phase equilibria and stability of ordered BCC phases in the Fe-rich portion of the Fe–Al system. Intermetallics **2001**, 9(9), 755-761. DOI: 10.1016/S0966-9795(01)00058-9.
16. Kim, H.; Suh, D. W.; Kim, N. J. Fe–Al–Mn–C lightweight structural alloys: a review on the microstructures and mechanical properties. Sci. Tech. Adv. Mater. **2013**, 14(1), 1-11. DOI: 10.1088/1468-6996/14/1/014205.
17. Frommeyer, G.; Bruex, U. Microstructures and mechanical properties of high-strength Fe-Mn-Al-C light-weight TRIPLEX steels. Steel research international **2006**, 77(9-10), 627-633 . DOI: 10.1002/srin.200606440

18. Sutou, Y.; Kamiya, N.; Umino, R.; Ohnuma, I.; Ishida, K. High-strength Fe-20Mn-Al-C-based alloys with low density. ISIJ international **2010**, 50(6), 893-899. DOI: http://doi.org/10.2355/isijinternational.50.893.
19. Greer, A. L.; Rutherford, K. L.; Hutchings, I.M; Wear resistance of amorphous alloys and related materials. International Materials Reviews **2002**, 47(2), 87-112. DOI: 10.1179/095066001225001067.
20. Maupin, H. E.; Wilson, R. D.; Hawk, J.A. Wear deformation of ordered Fe-Al intermetallic alloys. Wear **1993**, 162, 432-440. DOI: 10.1016/0043-1648(93)90527-S.
21. Xu, B.; Zhu, Z.; Ma, S.; Zhang, W.; Liu, W. Sliding wear behavior of Fe–Al and Fe–Al/WC coatings prepared by high velocity arc spraying. Wear **2004**, 257(11), 1089-1095. DOI: 10.1016/j.wear.2004.05.012.
22. Kim, Y. S.; Kim, Y. H. Sliding wear behavior of Fe 3 Al-based alloys. Mater. Sci. Eng. A **1998**, 258(1), 319-324. DOI: 10.1016/S0921-5093(98)00951-4.
23. Chonglin, W. Discussion on radial crushing strength testing. Powder Metallurgy Technology **1996**, 8, 206-211 .
24. Candela, N.; Plaza, R.; Rosso, M.; Velasco, F.; Torralba, J. M. Radial crushing strength and microstructure of molybdenum alloyed sintered steels. Journal of Materials Processing Technology **2001**, 119(1), 7-13. DOI: 10.1016/S0924-0136(01)00890-1 .
25. Larker, H. T.; Larker, R. Hot isostatic pressing. Materials Science and Technology **1991**. DOI: 10.1002/9783527603978.mst0201.
26. Leuenberger, H.; Rohera, B.D. Fundamentals of powder compression. I. The compactibility and compressibility of pharmaceutical powders. Pharmaceutical research **1986**, 3(1), 12-22. DOI: 10.1023/A: 1016364613722 .
27. Hryha, E.; Dudrova, E.; Bengtsson, S. Influence of powder properties on compressibility of prealloyed atomised powders. Powder Metallurgy **2008**, 51(4), 340-342. DOI: 10.1179/174329008X286596.
28. El-Hadek, M. A.; Kaytbay, S. H. Fracture properties of SPS tungsten copper powder composites. Metall. Trans. A **2013**, 44(1), 544-551. DOI: 10.1007/s11661-012-1396-x.
29. Kaytbay, S.; El-Hadek, M. Wear resistance and fracture mechanics of WC–Co composites. International Journal of Materials Research **2014**, 105(6), 557-565. DOI: 10.3139/146.111069.
30. El-Hadek, M. A.; Kassem, M. Failure behavior of Cu–Ti–Zr-based bulk metallic glass alloys. Journal of materials science **2009**, 44(4), 1127-1136. DOI: 10.1007/s10853-008-3194-9.
31. El-Hadek, M.; Kaytbay, S. Characterization of copper carbon composites manufactured using the electroless precipitation process. Materials and Manufacturing Processes **2013**, 28(9), 1003-1008. DOI: 10.1080/10426914.2012.736662.
32. El-Katatny, S. M.; Nassef, A. E.; El-Domiaty, A.; El-Garaihy, W.H. Fundamental Analysis of Cold Die Compaction of Reinforced Aluminum Powder. International Journal of Engineering and Technical Research **2015**, 3(3), 180-184. DOI: https://www.erpublication.org/published_paper/IJETR031605.pdf
33. Ahari, F. Flexible high radial strength stent. U.S. Patent 6, 264, 685, issued July 24, **2001**. DOI: file:///E:/1.%20My%20Drive/4.%20Research/Prof.%20Nassef/Fe-Al%20new/article/US6264685.pdf
34. Chtourou, H.; Guillot, M.; Gakwaya, A. Modeling of the metal powder compaction process using the cap model. Part I. Experimental material characterization and validation. International Journal of solids and Structures **2002**, 39(4), 1059-1075. DOI: 10.1016/S0020-7683(01)00255-4.
35. Bocchini, G.F. Warm compaction of metal powders: why it works, why it requires a sophisticated engineering approach. Powder Metallurgy **2013**, 42(2), 171-180. DOI: 10.1179/003258999665530.

36. Wang, J.; Xing, J.; Cao, L.; Su, W.; Gao, Y. Dry sliding wear behavior of Fe3Al alloys prepared by mechanical alloying and plasma activated sintering. Wear **2010**, 268(3), 473-480. DOI: 10.1016/j.wear.2009.09.006.
37. Sharma, G.; Limaye, P. K.; Ramanujan, R. V.; Sundararaman, M.; Prabhu, N. Dry-sliding wear studies of Fe 3 Al-ordered intermetallic alloy. Mater. Sci. Eng. A **2004**, 386(1), 408-414. DOI: 10.1016/j.msea.2004.07.053.
38. Dhokey, N. B.; Rane, K. K. Wear behavior and its correlation with mechanical properties of TiB_2 reinforced aluminium-based composites. Advances in Tribology **2011**, 2011**,** 1-8. DOI: http://dx.doi.org/10.1155/2011/837469.
39. Tong, C. J.; Chen, M.R.; Yeh, J.W.; Lin, S.J.; Chen, S. K.; Shun, T. T.; Chang, S. Y. Mechanical performance of the Al x CoCrCuFeNi high-entropy alloy system with multiprincipal elements. Metall. Trans. A **2005**, 36(5), 1263-1271. DOI: 10.1007/s11661-005-0218-9.
40. Hsu, C. Y.; Yeh, J. W.; Chen, S. K.; Shun, T. T. Wear resistance and high-temperature compression strength of Fcc CuCoNiCrAl0. 5Fe alloy with boron addition. Metall. Trans. A **2004**, 35(5), 1465-1469. DOI: 10.1007/s11661-004-0254-x.
41. Chen, M. R.; Lin, S. J.; Yeh, J. W.; Chuang, M. H.; Chen, S. K.; Huang, Y. S. Effect of vanadium addition on the microstructure, hardness, and wear resistance of Al0. 5CoCrCuFeNi high-entropy alloy. Metall. Trans. A **2006**, 37(5), 1363-1369. DOI: 10.1007/s11661-006-0081-3.